THE JOURNAL OF PHYSICAL CHEMISTRY Letters

Letter

pubs.acs.org/JPCL

Optimized Vertical Carbon Nanotube Forests for Multiplex Surface-Enhanced Raman Scattering Detection

Pola Goldberg-Oppenheimer,*[,†] Tanya Hutter,[‡] Bingan Chen,[†] John Robertson,[†] Stephan Hofmann,[†] and Sumeet Mahajan*[,§,∥]

[†]Department of Engineering, University of Cambridge, Cambridge CB3 0FA, United Kingdom

[‡]Department of Chemistry, University of Cambridge, Cambridge CB2 1EW, United Kingdom

[§]Department of Physics, Cavendish Laboratory, University of Cambridge, Cambridge CB30HE, United Kingdom

Supporting Information

ABSTRACT: The highly sensitive and molecule-specific technique of surface-enhanced Raman spectroscopy (SERS) generates high signal enhancements via localized optical fields on nanoscale metallic materials, which can be tuned by manipulation of the surface roughness and architecture on the submicrometer level. We investigate gold-functionalized vertically aligned carbon nanotube forests (VACNTs) as low-cost straightforward SERS nanoplatforms. We find that their SERS enhancements depend on their diameter and density, which are systematically optimized for their performance. Modeling of the VACNT-based SERS substrates confirms consistent dependence on structural parameters as observed experimentally. The created nanostructures span over large substrate areas, are readily configurable, and yield uniform and reproducible SERS enhancement factors. Further fabricated micropatterned VACNTs platforms are shown to deliver *multiplexed* SERS detection. The unique properties of CNTs, which can be synergistically utilized in VACNT-based substrates and patterned arrays, can thus provide new generation platforms for SERS detection.

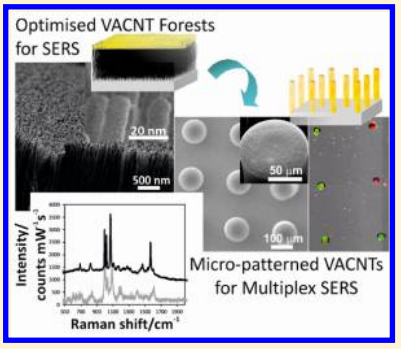

SECTION: Plasmonics, Optical Materials, and Hard Matter

Owing to its fingerprint molecular specificity and high sensitivity, surface-enhanced Raman scattering (SERS) is an established analytical tool for chemical and biological sensing[1] capable of single-molecule detection.[2,3] A strong Raman signal can be generated from SERS-active platforms given the analyte is within the enhanced plasmon field generated near a noble-metal nanostructured substrate. The key requirement for generating strong plasmon resonances to provide this electromagnetic enhancement is an appropriate metal surface roughness. Controlling nanoscale features for generating these regions of high electromagnetic enhancement, the so-called SERS "hot-spots", is still a challenge.[4] Significant advances have been made in SERS research, with wide-ranging techniques to generate substrates with tunable size and shape of the nanoscale roughness features.[4,5] Nevertheless, the development and application of SERS has been inhibited by the irreproducibility and complexity of fabrication routes. The ability to generate straightforward, cost-effective, multiplex-able and addressable SERS substrates with high enhancements is of profound interest for SERS-based sensing devices.

Carbon nanotubes (CNTs) have been, concurrently, a topic of extensive research and applications, in particular because of their extraordinary electrical, thermal, and mechanical properties.[6−12] However, the application of CNTs for plasmonics including SERS has been only recently beginning to gain interest.[13−17] These studies use *nanoparticle*-functionalized CNTs for SERS and consequently their reproducibility and stability, and hence their practical applications remain debatable. Recently, Milne and coworkers reported the modeling and use of large diameter multiwalled carbon nanotubes (MWNTs) coated with silver as antennae for enhancing Raman signals,[18] although for practical SERS applications, gold coating, being more inert and stable, is more suitable compared to silver. However, none of the studies have paid attention to the structural parameters for optimization of CNT-based substrates for SERS. Control and understanding of the role of structural parameters for the generation of "hot-spots" is necessary to take full advantage of the synergistic functions of CNT-based SERS architectures. Furthermore, the utilization of VACNT forests for SERS remains rather unexplored. VACNTs can provide low-cost, simple, large-active-area patternable substrates which, through appropriate functionalization, will be able to provide advanced SERS platforms.

In the present work, we fabricate gold-functionalized VACNT forests and investigate Raman signal strength with variation in diameter of nanotubes and their spacing to deliver optimized multiplex SERS substrates. The dependence on the

Received: September 3, 2012
Accepted: November 12, 2012
Published: November 12, 2012

   dx.doi.org/10.1021/jz301333r | *J. Phys. Chem. Lett.* 2012, 3, 3486−3492

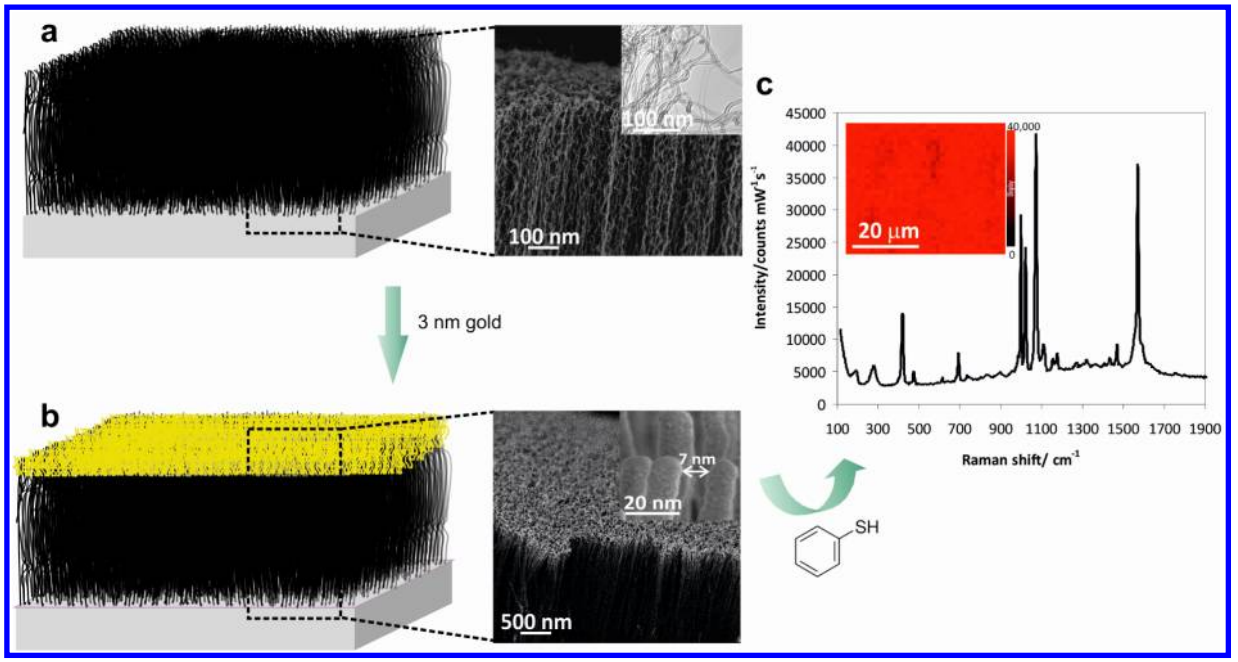

Figure 1. Fabrication of well-ordered large-area VACNTs-Au SERS-active platforms. Schematic and corresponding SEM images in set contrast show CVD grown CNTs forests (a), which are then coated with a 3 nm Au layer (b) to yield stable surfaces with high SERS enhancement. TEM characterization reveals CNTs with a diameter of 8 ± 1.5 nm (a, inset). Low-angle back-scattered cross-sectional SEM images of gold coated (b) are clearly distinct from bare (a) VACNT forests, as seen from a zoomed-in SEM image of the individual CNTs tip coated with Au film (b, inset). (c) Representative spectrum of benzenethiol recorded from Au-coated VACNTs SERS substrate shown in panel b. For control spectra, see Figure S6 of the Supporting Information. The inset in panel c shows a SERS map recorded with 633 nm excitation, reconstructed using the intensity of the 1070 cm^{-1} peak, overlaid over of a scanned area showing the uniformity of signals.

VACNTs' diameters and density is found to play an important role in Raman enhancements, thus highlighting the importance of structural parameters, previously overlooked in designing and fabricating optimized CNTs-based SERS nanoprobes. Smaller diameter and higher density VACNT forests yield stronger relative enhancement. The diameter of CNTs, their height, and the density (i.e., average separation between CNTs) can be tuned by regulating the VACNT growth process conditions. The configurability of CNT substrates can be utilized to fabricate substrates with the highest and most uniform SERS signals. These large-surface-area substrates demonstrate remarkable SERS enhancement factors, up to 10^7 due to the high concentration of hot-spots provided by the VACNT forests. Gold-coated small-diameter VACNT forests patterned into predesigned pillar structures are further utilized for duplex detection, demonstrating that patterned VACNT arrays can act as straightforward and cost-effective substrates for high-throughput multiplex SERS detection. Because vertically oriented CNTs exhibit functionalities such as electrical conductivity and unique adsorption properties, these can be further harnessed in their development as novel chemical and biosensing platforms.

The procedure for the fabrication of SERS-active nanotube forests is illustrated in Figure 1. Vertically oriented CNTs with varying diameters (between 5 and 15 nm) and site densities in the range of 7−30% coverage grown via CVD process (see the Experimental Section and Supporting Information, S1 for details) yield well-defined stable large area substrates of nanotube arrays (Figure 1a). To transform the bare VACNT arrays into SERS active platforms, we coated the structures with a 3 nm thick gold layer (Figure 1b and Figures S2 and S3 of the Supporting Information). The corresponding low-angle back-scattered scanning electron microscopy (LAB-SEM) images of the uncovered CNTs platforms (Figure 1a, right) and the Au-coated VACNT substrates (Figure 1b, right) clearly confirm that the tips of the nanotubes are covered uniformly up to ∼300 nm (avg. l_{Au} = 295 ± 70 nm) with a thin layer of gold (also see S2 of the Supporting Information).

These generated VACNTs-Au substrates are vertically aligned over a large area (5 × 5 mm^2) and thus provide stable platforms with a high concentration of "hot-spots" enabling SERS detection. With normal excitation, with polarization perpendicular to axial direction, the length of the nanotubes is unlikely to contribute toward surface enhancement. To assess the SERS performance of VACNTs-Au structures shown in Figure 1a,b, a benzenethiol monolayer was adsorbed on these substrates. A representative SERS spectrum recorded for these pillar-like CNT structures (average diameter of 8.0 ± 1.5 nm (Figure 1a, inset)) is shown in Figure 1c. Under the experimental conditions (low excitation power of 0.3 mW) peaks corresponding only to the adsorbed benzenethiol molecules are visible. The absolute enhancement factor is calculated to be ∼1.0 × 10^7 with a 95% confidence interval of 8.93 × 10^6 to 1.07 × 10^7. Note that these enhancement factors are normalized by illuminated area (spot size) while the SERS activity is localized at the surface structure and therefore stems only from a small fraction of the sample area. In addition to spectroscopic data collection, SERS mapping was carried out on these substrates. A representative SERS map overlaid on its corresponding optical image is shown in Figure 1c. The SERS signal (red) comes directly from the gold-covered CNTs and it displays spectral homogeneity over the area of examined surface.

A range of VACNT configurations can be accomplished by modification of experimental parameters. VACNTs with varying densities and diameters were grown and SERS

dx.doi.org/10.1021/jz301333r | J. Phys. Chem. Lett. 2012, 3, 3486−3492

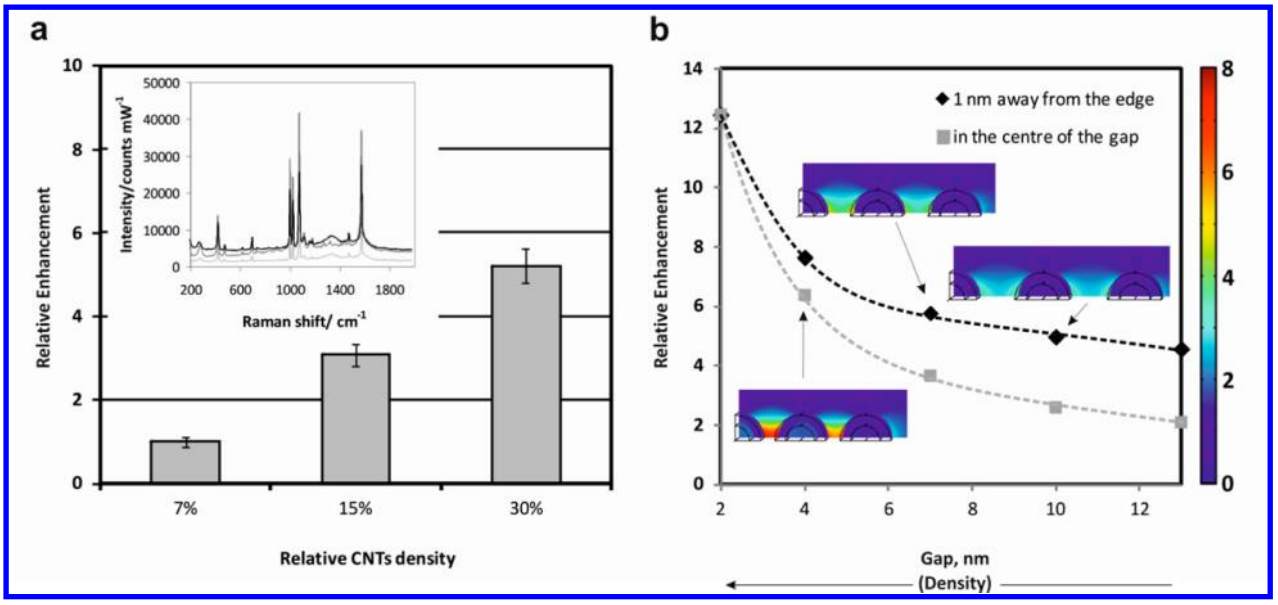

Figure 2. VACNTs-Au substrates configurability versus SERS enhancement. (a). The relative enhancement for the 1070 cm^{-1} benzenethiol peak recorded on three different substrates with varying nanotube forest densities. SERS measurements were done with a 633 nm laser. The inset shows representative SERS spectra for the three corresponding VACNTs-Au forests densities. (b) Simulated field enhancement $|E|/|E_0|$ of 8 nm diameter CNT for various gaps. The relative enhancement (i.e., average enhancement) values are shown in the center of the gap and 1 nm away from the gold coated CNT. Field distribution and enhancement levels were similar at z_{top} and z_{mid}. In the insets, the top-view of spatial field distributions are shown for a gap of 4, 7, and 10 nm.

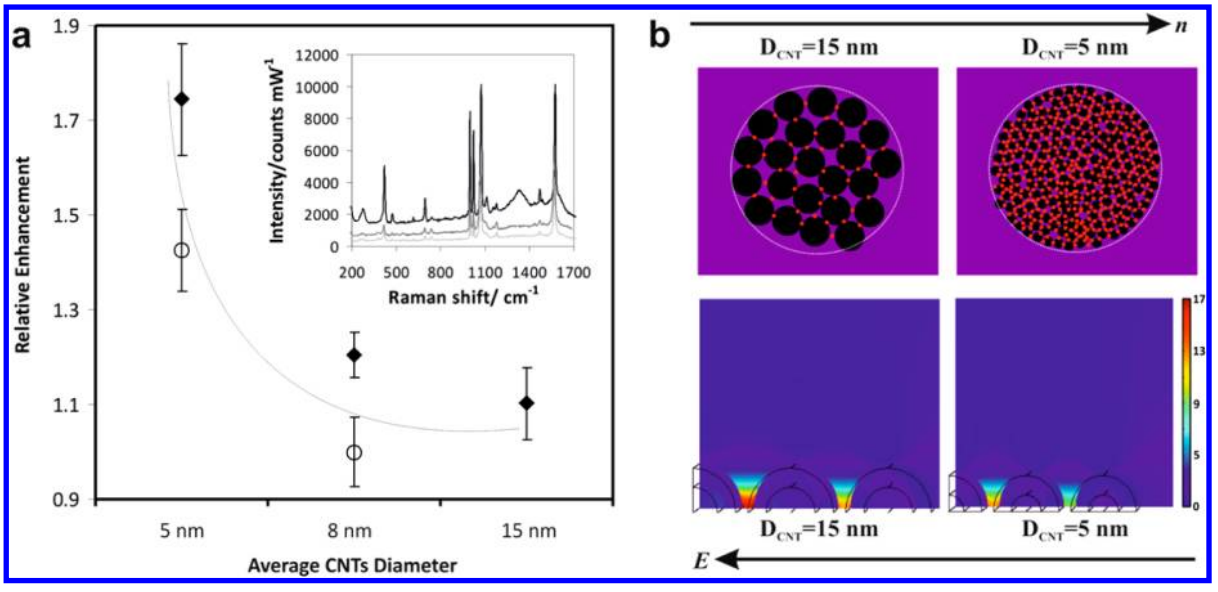

Figure 3. (a). Relative enhancement dependence on nanotube diameters with the corresponding SERS spectra recorded on substrates with different VACNTs diameters at constant (highest) forest density shown in inset. Both normal (black diamonds) and inverted CNTs (white circles) have been examined as SERS substrates. The inset shows representative SERS spectra with the three corresponding normal (as-grown) CNTs diameters. SERS measurements were done with a 633 nm laser. (b). Schematic illustration of the density of hot spots for two CNT diameters (upper row) and its corresponding spatial field distribution (lower row) at a constant site density (i.e., constant gap distance). In our simulations, the field enhancements are higher in gaps between nanorods, which are toward the center as a result of optical coupling between them.

substrates were fabricated with them. Note that the direct characterization of the precise nanotube area density is difficult and is typically given as site density values. Of the three well-accepted methods used to measure this parameter,[19] the most quantitative weight-gain method was employed in this study (see Supporting Information for details, S1). In subsequent paragraphs, we describe the effect of variation in density of CNTs and their diameter on SERS enhancements.

We find that the SERS enhancements increase with the site density of VACNT arrays (Figure 2a). The increase in the density of VACNTs-Au arrays results in a diminished intertube spacing, with the gaps between neighboring tubes of a few nanometers only. The efficient coupling of the localized surface plasmons at increased VACNTs density also arises from the increase in the "hot spots" generated by the sub-10 nm gaps between them. The SERS response is therefore dominated by the highly localized plasmon modes created by strong

dx.doi.org/10.1021/jz301333r | J. Phys. Chem. Lett. 2012, 3, 3486−3492

electromagnetic coupling between the metallized CNTs. We have further simulated a 3D model of gold-coated CNTs using a finite-element method, where the incident plane wave propagates at normal incidence with a linear polarization perpendicular to the nanorods length axis. The scattered electric field generated by the gold coated CNTs in vacuum is simulated for various gaps and CNT's radii (see Experimental Section for further details). These simulations provide an indication of how the gaps between the nanorods and their size affect the relative field enhancement that they generate. Indeed, from the simulations in Figure 2b, the coupling between the gold-coated CNTs increases as the gap between them is reduced; therefore, at higher densities we observe relatively higher SERS signals. This is consistent with the gap dependence for plasmon coupling between spherical nanoparticle dimers[20] and chains creating nanojunctions.[21]

However, for the same site density of CNTs, larger diameters yield ~36% lower SERS enhancement factors (Figure 3a). For the similar growth conditions, the larger diameter tubes result in much fewer junctions, n (inversely proportional to the square of the diameter), and hence the number of molecules between the tubes ("hot spots") in a given area. However, less than 50% reduction is observed on going from a diameter of 5 to 15 nm (Figure 3b) while n decreases 900% (nine times). This is explained by an increased optical coupling efficiency of larger diameter tubes as their plasmon resonance increasingly couples to the excitation laser. Larger diameter tubes are expected to have larger scattering cross sections and their LSPR (localized surface plasmon resonance) is expected to red-shift. Both of these factors can help in increased coupling with the excitation laser. We confirm this by simulations of the CNT arrays (Figure 3b and also see Supporting Information, S6) which predict that with increasing diameters the electric field enhancement $|E|/|E_0|$ increases until a CNT diameter of 10 nm and then decreases. This is due to the red shift of plasmon resonances as the diameter increases, which ultimately ceases to be in resonance with the laser excitation for diameters larger than 10 nm. Nevertheless, as a consequence of these two counteracting effects, (Figure 3b) SERS enhancements show only a moderate decrease with increased CNTs diameters (Figure 3a).

The above-discussed enhancement factors were measured from as-grown anisotropic carbon nanotube arrays with typical top-surface consisting of curly entangled nanotube ends (Figure 4). To investigate whether the removal of the nonaligned nanotube segments yields stronger enhancement, we flipped over the as-grown VACNTs (see Experimental Section), exposing better defined nanotube tips (see Figure 4, inset). The inverted CNTs forests were also coated with a 3 nm thick gold layer, followed by adsorption of benzenethiol for recording SERS spectra with these structures. The inverted VACNTs do not show a significant difference in SERS enhancements and show a similar trend to the as-grown substrates. The slightly lower values obtained for the inverted tubes could be on account of fewer contacts between them because of their well-aligned nature. However, for computational simplicity, only the well-aligned nanorods were simulated, as previously described, and the experimental results for them correlate well with calculations.

SERS signal reproducibility of the VACNTs-Au platforms was subsequently tested by examining three to seven different areas across the substrate under identical experimental conditions as well as across different substrates. Good signal reproducibility was found for each substrate and between substrates with <15% variation in all cases (also indicated by error bars in Figures 2 and 3; see Supporting Information S4).

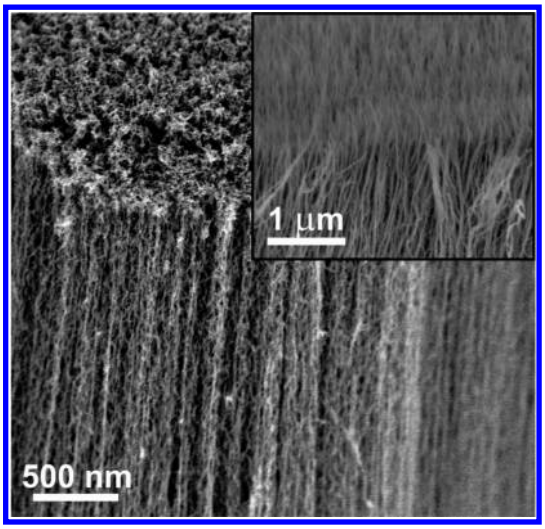

Figure 4. Cross-sectional SEM view of the as-grown VACNTs and inverted forests (inset) with straighter nanotubes endings.

Furthermore, various VACNTs-based SERS nanostructures can be designed and fabricated by prewriting the location and dimensions of CNT growth areas. Herein we have fabricated SERS-active substrates using electron beam lithography generated patterns of an array of pillars for detection of multiple analytes. VACNTs (average diameter 8.0 ± 1.5 nm) were grown into arrays with predesigned dimensions of 100 μm diameter with a 250−500 μm pitch between the individual pillars (Figure 5a). A thin gold layer was evaporated onto the pillar CNT-based structures (Figure 5b), and monolayers of various molecules were adsorbed on different SERS-active pillars. An illustration of the generation of such VACNT-based SERS platforms and their utilization in multiplex targeting is shown in Figure 5a−c. Two different molecules were spotted on adjacent pillars using position-controlled micropipettes. In this proof-of-concept duplex detection, pyridinethiol and benzenethiol were easily detected using SERS mapping due to their different spectral signatures (Figure 5c). Pyridinethiol signals were weaker than those of benzenethiol, and this could be attributed to their SERS cross sections or the so-called "chemical effect".

The fabrication of well-designed, optimized SERS-active arrays is useful to analyze a variety of mixtures involved in environmental and biological sensing. Whereas current demonstration uses different components spotted beforehand on the array, targeted functionalization of different pillars will allow in situ detection. Each individual structure in the array could be specifically functionalized with receptors for different molecules for multiplexed detection. Furthermore, we envisage other techniques such as using photolithographic masks and templates combined with metal deposition to generate a master for producing replicated architectures to be equally feasible to generate CNT-based SERS arrays. Finally, oriented VACNTs exhibit high electrical conductivity and can provide an electrochemically accessible surface area. This is potentially useful for the development of rapid-response addressable biochemical sensors that are selective for targeted chemical and biological molecules.

dx.doi.org/10.1021/jz301333r | J. Phys. Chem. Lett. 2012, 3, 3486−3492

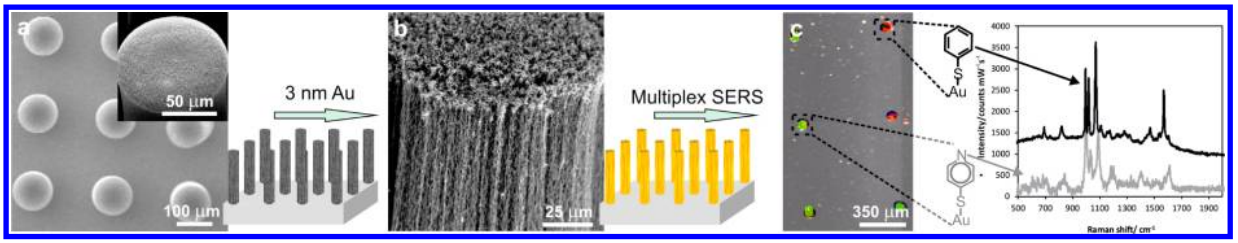

Figure 5. Platforms for multiplex SERS detection. (a,b) SEM images of as-fabricated and covered with Au nanolayer VACNT pillar arrays with corresponding schematic diagrams. (c) SERS map image reconstructed using representative peaks of the two components attached to adjacent pillars showing duplex detection. The map was reconstructed using the sum intensities of the distinct representative peaks of pyridinethiol (green) and benzenethiol (red). Inset: SERS spectra of the two components detected are shown. Pyridinethiol (gray) with distinct representative peaks at 1090, 1209, and 1605 cm^{-1} compared with benzenethiol (black), which has peaks at 1000, 1021, 1070, and 1572 cm^{-1}.

In conclusion, the use of gold-coated VACNT forests as SERS substrates has been shown to deliver high reproducible enhancements of the order of 10^7 and over large areas of 5 × 5 mm^2 and above. The enhancement properties of the VACNTs-Au SERS substrates have found to be highly dependent on the structural parameters of the CNTs, such as diameter and distance. These factors are configured using straightforward process control (i.e., control of the catalyst or growth conditions). VACNTs with an increased relative density and smaller diameters yield higher Raman signal enhancements. Therefore, by altering the above key parameters VACNTs gold-coated substrates can be tuned and tailored to provide advanced applications. Furthermore, the dependence of SERS enhancements is verified and found to be consistent with EM simulations. Finally, we have shown that patterned arrays of CNTs can be fabricated to give multiplexed SERS detection. Such unique combination of materials and nanospectroscopic platforms is promising for a variety of applications in chemical and biological sensing.

EXPERIMENTAL METHODS

Growth of the VACNT Forests. CNT arrays were grown on the 5 × 5 mm^2 substrates, utilizing cold-wall system of the catalytic chemical vapor deposition (CVD) process.[22] Silicon substrates were sputtered with a catalyst layer consisting of Al_2O_3 buffer and Fe catalysts. During the growth process, initially 500 sccm of H_2 was heated to 750 °C at 5 min under controlled system pressure of 15 mbar. CNTs growth proceeded at 750 °C with a gas flow of H_2:C_2H_2 (460:40 sccm). Once the growth was completed, the sample was cooled to room temperature under the flow of 500 sccm H_2.

Fabrication of Patterned CNTs Arrays. CNTs arrays were fabricated using an electron beam (e-beam) lithography combined with CVD growth process. Initially, a layer of photoresist (UVIII) was spin-coated on a silicon substrate and further annealed at 120 °C for 2 min. Following this, the resist was exposed under the e-beam with (pre)-written dimensions for the generated patterns (i.e., 100 μm diameter pillars with spacing of 700 μm). Finally, it was postbaked at 140 °C for 2 min and developed in CD26 for 30 s, and the patterned pillar arrays were obtained. These written structures were further filled by depositing 10 nm alumina (i.e., used as a buffer layer) and 1.3 nm iron (i.e., catalysts) through sputtering process, followed by lifting off the resist from acetone. CVD process was applied using a combination of H_2:C_2H_2 (70:30 sccm) at 750 °C for 2 min. Pillar CNTs arrays with desired dimensions were ultimately grown on top of the patterned catalysts.

Variation of CNT Forests Densities. CNTs with different densities were obtained by varying the catalysts and their dimensions for CVD growth (see Supporting Information S1 for further details). The densities of the CNTs forests were obtained by using liquid-induced collapse approach[19] using isopropanol (IPA), causing an aggregation of the CNTs.

Generation of Inverted CNT Forests. The as-grown CNTs were transferred to poly(methyl methacrylate) (PMMA) using the previously established procedure.[23] Initially, a homogeneous PMMA layer was spin-cast on a silicon wafer, followed by placing the VACNTs forest on top (i.e., facing the PMMA film) and annealing at 180 °C for 1 min. The sample was allowed to cool to the RT (i.e., below the glass-transition temperature of the polymer film), resulting in a solidification of the film while embedding the upper ends of the CVD-grown CNTs forest. The CNTs were further peeled off the (original) silicon substrate, exposing more straight ends.

Characterization. The scanning electron microscopy (SEM) measurements were performed using a LEO ULTRA 55 SEM including a Schottky emitter (ZrO/W cathode) at acceleration voltages of 1−5 KV with a lateral resolution of 2−5 nm. Scanning transmission electron microscope (STEM) images were obtained using Hitachi s5500 with a cold field-emission source and lens detector with 4 Å resolution, allowing adjustable acceptance angle STEM imaging. Low-angle back-scattered electrons imaging mode was used to contrast the noncoated VACNTs and those sputtered with gold, providing the atomic number contrast.

SERS Measurements. SERS measurements were carried out with an InVia Renishaw Raman Microscope System equipped with 633 nm laser. The spectra were typically acquired with a 10 s exposure time and a laser power of 0.3 mW at the sample at 633 nm. SERS maps were acquired in Streamline mode (line scan) with 5 s of exposure time per pixel and a power of 6 mW with a 633 nm laser. A 100× objective with a numerical aperture of 0.85 was used for all measurements.

Numerical Simulations. A 3D model using COMSOL Multiphysics v4.3, a commercial finite-element mode solver, was constructed to enable parametric studies. The simulation was done for five nanorods in a line, where each nanorod is a CNT-coated nanotube with 3 nm of gold. Their simulated length was 50 nm. Optical constants of the gold were taken from ref 24, and those of the CNT were taken from ref 25. The incident field (wavelength 633 nm) propagates from the top in the $-z$ direction, with linear polarization in the x direction. The incident field amplitude is E_0 = 1 V/m. The model was solved for the scattered field of the nanorods in vacuum. The total width, depth, and height of the model were 400, 600, and 300 nm. Perfectly matched layers (PMLs) were used to absorb the scattered radiation in all directions; their thickness was 50 nm. A sufficiently small mesh (0.3 nm) has been used at the gaps

dx.doi.org/10.1021/jz301333r | J. Phys. Chem. Lett. 2012, 3, 3486−3492

compared with the bulk of the model, where the maximum mesh size was set to 25 nm. To reduce the computational time, symmetry planes were used, and thus the field was solved for only one-quarter of the model. The field intensity was taken either in the middle of the gap between the nanorods or 1 nm away from the nanorods. In both cases, two points were examined: point at the height of the rods (z_{top}) and in the middle height (z_{mid}).

■ ASSOCIATED CONTENT

Supporting Information

Further particulars regarding the measurement of CNTs forests' site density, roughness and conformal coverage of the deposited gold layer, reproducibility of VACNTs-Au SERS substrates, calculation of the SERS enhancement factor, and numerical simulations of the enhancement versus the CNTs diameter variation and control data (blanks) on VACNT and benzenethiol-free gold coated VACNT SERS substrates. This material is available free of charge via the Internet at http://pubs.acs.org.

■ AUTHOR INFORMATION

Corresponding Author

*Tel: +44 (0)1223 748317; Fax: +44 (0)1223 748293; E-mail: pg333@cam.ac.uk (P.G.-O.). Tel: +44 (0)1223 746931; Fax: +44 1223 337000; E-mail:sm735@cam.ac.uk (S.M.).

Present Address

[‖]Institute of Life Sciences and Department of Chemistry, University of Southampton, SO17 1BJ, United Kingdom. Tel: +44 (0)2380 597747.

Funding

We acknowledge funding from EPSRC (EP/G060649/1, EP/H028757/1).

Notes

The authors declare no competing financial interest.

■ ACKNOWLEDGMENTS

We appreciate the guidance of J. J. Rickard with electron microscopy analysis.

■ REFERENCES

(1) Bartlett, P.; Mahajan, S.: Raman Spectroscopy of Biomolecules at Electrode Surfaces. In *Advances in Electrochemical Science and Engineering*; Wiley-VCH Verlag: Weinheim, Germany, 2011; pp 269−334.

(2) Kneipp, K.; Wang, Y.; Kneipp, H.; Perelman, L. T.; Itzkan, I.; Dasari, R. R.; Feld, M. S. Single Molecule Detection Using Surface-Enhanced Raman Scattering (SERS). *Phys. Rev. Lett.* **1997**, *78*, 1667−1670.

(3) Nie, S.; Emory, S. R. Probing Single Molecules and Single Nanoparticles by Surface-Enhanced Raman Scattering. *Science* **1997**, *275*, 1102−1106.

(4) Baker, G. A.; Moore, D. S. Progress in Plasmonic Engineering of Surface-Enhanced Raman Scattering Substrates Toward Ultra-Trace Analysis. *Anal. Bioanal. Chem.* **2005**, *382*, 1751−1770.

(5) Fan, M.; Andrade, G. F. S.; Brolo, A. G. A Review on the Fabrication of Substrates for Surface Enhanced Raman Spectroscopy and their Applications in Analytical Chemistry. *Anal. Chim. Acta* **2011**, *693*, 7−25.

(6) Baughman, R. H.; Zakhidov, A. A.; de Heer, W. A. Carbon Nanotubes–The Route Toward Applications. *Science* **2002**, *297*, 787−792.

(7) Sun, Y.-P.; Fu, K.; Lin, Y.; Huang, W. Functionalized Carbon Nanotubes: Properties and Applications. *Acc. Chem. Res.* **2002**, *35*, 1096−1104.

(8) Dresselhaus, M. S.; Dresselhaus, G.; Jorio, A. Unusual Properties and Structue of Carbon Nanotubes. *Ann. Rev. Mater. Res.* **2004**, *34*, 247−278.

(9) Qu, L.; Vaia, R. A.; Dai, L. Multilevel, Multicomponent Microarchitectures of Vertically-Aligned Carbon Nanotubes for Diverse Applications. *ACS Nano* **2011**, *5*, 994−1002.

(10) Kinoshita, H.; Kume, I.; Tagawa, M.; Ohmae, N.; Turq, V.; Martin, J. M. Microtribological Property of Vertically Aligned Carbon Nanotube Film. In *IDans Synopses of the International Tribology Conference Kobe, 2005 - International Tribology Conference, Kobe: Japan (2005)*, 2008.

(11) Lim, S. C.; Jeong, H. J.; Park, Y. S.; Bae, D. S.; Choi, Y. C.; Shin, Y. M.; Kim, W. S.; An, K. H.; Lee, Y. H. Field-Emission Properties of Vertically Aligned Carbon-Nanotube Array Dependent on Gas Exposures and Growth Conditions. *J. Vac. Sci. Technol., A* **2001**, *19*, 1786−1789.

(12) Miyake, K.; Kusunoki, M.; Usami, H.; Umehara, N.; Sasaki, S. Tribological Properties of Densely Packed Vertically Aligned Carbon Nanotube Film on SiC Formed by Surface Decomposition. *Nano Lett.* **2007**, *7*, 3285−3289.

(13) Beqa, L.; Singh, A. K.; Fan, Z.; Senapati, D.; Ray, P. C. Chemically Attached Gold Nanoparticle−Carbon Nanotube Hybrids for Highly Sensitive SERS Substrate. *Chem. Phys. Lett.* **2011**, *512*, 237−242.

(14) Wang, X.; Wang, C.; Cheng, L.; Lee, S.-T.; Liu, Z. Noble Metal Coated Single-Walled Carbon Nanotubes for Applications in Surface Enhanced Raman Scattering Imaging and Photothermal Therapy. *J. Am. Chem. Soc.* **2012**, *134*, 7414−7422.

(15) Chu, H.; Wang, J.; Ding, L.; Yuan, D.; Zhang, Y.; Liu, J.; Li, Y. Decoration of Gold Nanoparticles on Surface-Grown Single-Walled Carbon Nanotubes for Detection of Every Nanotube by Surface-Enhanced Raman Spectroscopy. *J. Am. Chem. Soc.* **2009**, *131*, 14310−14316.

(16) Chen, Y.-C.; Young, R. J.; Macpherson, J. V.; Wilson, N. R. Single-Walled Carbon Nanotube Networks Decorated with Silver Nanoparticles: A Novel Graded SERS Substrate. *J. Phy. Chem. C* **2007**, *111*, 16167−16173.

(17) Sun, Y.; Liu, K.; Miao, J.; Wang, Z.; Tian, B.; Zhang, L.; Li, Q.; Fan, S.; Jiang, K. Highly Sensitive Surface-Enhanced Raman Scattering Substrate Made from Superaligned Carbon Nanotubes. *Nano Lett.* **2010**, *10*, 1747−1753.

(18) Dawson, P.; Duenas, J. A.; Boyle, M. G.; Doherty, M. D.; Bell, S. E. J.; Kern, A. M.; Martin, O. J. F.; Teh, A. S.; Teo, K. B. K.; Milne, W. I. Combined Antenna and Localized Plasmon Resonance in Raman Scattering from Random Arrays of Silver-Coated, Vertically Aligned Multiwalled Carbon Nanotubes. *Nano Lett.* **2011**, *11*, 365−371.

(19) Zhong, G.; Warner, J. H.; Fouquet, M.; Robertson, A.; Chen, B.; Robertson, J. Growth Of Ultrahigh Density Single-Walled Carbon Nanotube Forests By Improved Catalyst Design. *ACS Nano* **2012**, *6*, 2893−2903.

(20) Halas, N. J.; Lal, S.; Chang, W.-S.; Link, S.; Nordlander, P. Plasmons in Strongly Coupled Metallic Nanostructures. *Chem. Rev.* **2011**, *111*, 3913−3961.

(21) Harris, N.; Arnold, M. D.; Blaber, M. G.; Ford, M. J. Plasmonic Resonances of Closely Coupled Gold Nanosphere Chains. *J. Phys. Chem. C* **2009**, *113*, 2784−2791.

(22) Zhong, G.; Hofmann, S.; Yan, F.; Telg, H.; Warner, J. H.; Eder, D.; Thomsen, C.; Milne, W. I.; Robertson, J. Acetylene A Key Growth Precursor for Single-Walled Carbon Nanotube Forests. *J. Phys. Chem. C* **2009**, *113*, 17321−17325.

(23) Sansom, E. B.; Rinderknecht, D.; Gharib, a. M. Controlled Partial Embedding of Carbon Nanotubes Within Flexible Transparent Layers. *Nanotechnology* **2008**, *19*, 035302.

(24) Johnson, P. B.; Christy, R. W. Optical Constants of the Noble Metals. *Phys. Rev. B* **1972**, *6*, 4370−4379.

(25) deHeer, W. A.; Bacsa, W. S.; Châtelain, A.; Gerfin, T.; Humphrey-Baker, R.; Forro, L.; Ugarte, D. Aligned Carbon Nanotube Films: Production and Optical and Electronic Properties. *Science* **1995**, *268*, 845−847.